The Astrophysical Journal, 835:195 (6pp), 2017 February 1 doi:10.3847/1538-4357/835/2/195

AstroSat/LAXPC Observation of Cygnus X-1 in the Hard State

Ranjeev Misra[1], J S Yadav[2], Jai Verdhan Chauhan[2], P C Agrawal[3], H M Antia[2], Mayukh Pahari[1], V R Chitnis[2], Dhiraj Dedhia[2], Tilak Katoch[2], P. Madhwani[2], R K Manchanda[4], B Paul[5], and Parag Shah[2]
[1] Inter-University Centre for Astronomy and Astrophysics, Pune 411007, India; rmisra@iucaa.in
[2] Tata Institute of Fundamental Research, Homi Bhabha Road, Mumbai, India
[3] UM-DAE Center of Excellence for Basic Sciences, University of Mumbai, Kalina, Mumbai-400098, India
[4] University of Mumbai, Kalina, Mumbai-400098, India
[5] Dept. of Astronomy & Astrophysics, Raman Research Institute, Bengaluru-560080, India
Received 2016 October 4; revised 2016 December 20; accepted 2016 December 27; published 2017 January 31

Abstract

We report the first analysis of data from *AstroSat*/LAXPC observations of Cygnus X-1 in 2016 January. LAXPC spectra reveals that the source was in the canonical hard state, represented by a prominent thermal Comptonization component having a photon index of ∼1.8 and high temperature of $kT_e > 60$ keV along with weak reflection and possible disk emission. The power spectrum can be characterized by two broad lorentzian functions centered at ∼0.4 and ∼3 Hz. The rms of the low-frequency component decreases from ∼15% at around 4 keV to ∼10% at around 50 keV, while that of the high-frequency one varies less rapidly from ∼13.5% to ∼11.5% in the same energy range. The time lag between the hard (20–40 keV) and soft (5–10 keV) bands varies in a step-like manner being nearly constant at ∼50 milliseconds from 0.3 to 0.9 Hz, decreasing to ∼8 milliseconds from 2 to 5 Hz and finally dropping to ∼2 milliseconds for higher frequencies. The time lags increase with energy for both the low and high-frequency components. The event mode LAXPC data allows for flux resolved spectral analysis on a timescale of 1 s, which clearly shows that the photon index increased from ∼1.72 to ∼1.80 as the flux increased by nearly a factor of two. We discuss the results in the framework of the fluctuation propagation model.

Key words: accretion, accretion disks – black hole physics – X-rays: binaries – X-rays: individual (Cyg X-1)

1. Introduction

Over the last several decades, the persistent black hole system, Cygnus X-1, has been a primary target of nearly all the X-ray observatories. Its brightness and persistent nature makes it the ideal choice to understand the behavior of black hole systems. Indeed, some of the earliest paradigms were based on observations of Cygnus X-1 such as the concept of a hot inner flow where the thermal plasma Comptonizes photons from a truncated standard disk producing the characteristic hard spectrum (Shapiro et al. 1976) and even the alternative that the spectrum is produced by a corona on top of an accretion disk (Liang & Price 1977). The various black hole system spectral states that are now known (e.g., Remillard & McClintock 2006) can be said to be inspired by the early classification of the spectra of Cygnus X-1 into hard and soft states (e.g., Thorne & Price 1975).

Although Cygnus X-1 is a persistent high mass X-ray binary, it shares several common spectral and timing features with other low mass X-ray binaries that harbor black holes. For example, its hard state spectrum can be represented approximately by being dominated by a hard power law with a high-energy cutoff, with weak reflection and disk components, which is also true for other black hole systems. As mentioned above, such a hard state spectrum is consistent with the picture of a truncated standard accretion disk with a hot inner region giving rise to the standard paradigm regarding the hard state geometry (Shapiro et al. 1976). However, with the availability of high-resolution spectra from *Suzaku* and *Nustar*, this paradigm is now being challenged. Apart from absorption effects due to the ionized wind, the hard state spectra of Cygnus X-1 show a relativistically broadened Iron line, which indicates that the standard disk is not truncated but extends all the way to the last stable orbit (Parker et al. 2015). Such broad lines have also been reported for the luminous hard state of another black hole system GX 339-4 (Plant et al. 2015), suggesting that the geometry of the system may depend on the luminosity of the hard state. Along with such detailed spectral studies, it is important to consider the timing properties of these sources to pin down the true geometry and nature of these sources.

The *Rossi X-ray Timing Experiment* (*RXTE*) has revolutionized our understanding of the high-frequency variability of black hole systems. It is not surprising that one of the pioneering works, where the application of timing analysis such as coherence, energy, and frequency dependent time lags were introduced, was an analysis of early *RXTE* data of Cygnus X-1 (Nowak et al. 1999). Since then, a large number of analyses have been undertaken on several *RXTE* data sets of Cygnus X-1, and now results of comprehensive timing analysis using nearly all *RXTE* observations of the source are available (e.g., Wilms et al. 2004).

RXTE analyses have shown that for the hard state the variability of Cygnus X-1 is primarily between ∼0.1 and ∼10 Hz and its power spectrum can be approximately described by two to four broad lorentzians in this frequency range (e.g., Nowak et al. 1999; Wilms et al. 2004). Time lag of high-energy photons with respect to the low-energy ones are known to approximately increase linearly with the logarithm of the energy. The lags decrease as a function of frequency roughly as a power law. Cygnus X-1 is known to show a linear relation between flux and rms (Uttley & McHardy 2001; Gleissner et al. 2004), which is now known as the universal flux–rms relation applicable to several X-ray binaries and Active Galactic Nuclei. Another related nearly universal property of these systems, that the flux distribution is a log-normal one, was first shown for Cygnus X-1 (Uttley et al. 2005).

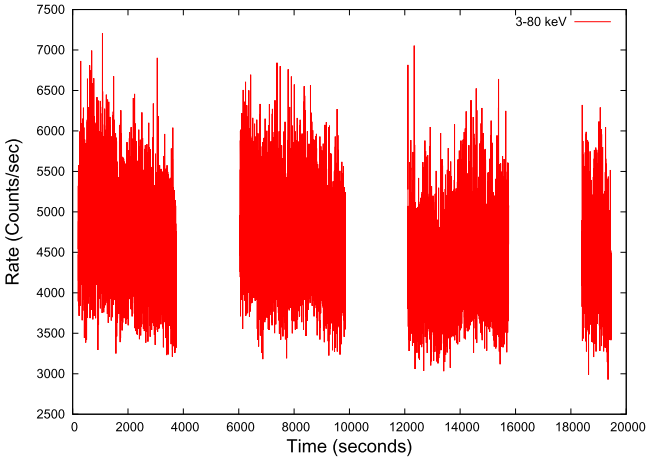

Figure 1. Light curve of Cygnus X-1 in the energy range of 3–80 keV is shown where the count rate from all three LAXPC detectors—LAXPC 10, LAXPC 20, and LAXPC 30 are combined. The gaps are due to SAA or earth occultations.

The timescales of the variability as well as those of the time lags are significantly longer than the light crossing time of the inner regions of the accretion disk. This indicates that the variability is related to the viscous timescale suggesting an origin in the outer regions of the disk. However, the variability is observed in hard X-rays, which originate from the inner regions. An explanation was provided by Lyubarskii (1997), where the accretion disk undergoes stochastic variations all across the disk and the fluctuations propagate inward reaching the inner disk after a viscous timescale corresponding to their origin. Since the different fluctuations have a multiplicative effect on the inner regions, the model can naturally explain the flux–rms relation as well as the log-normal distribution of the flux. Moreover, the time lags as a function of energy and frequency have a natural explanation in this framework (e.g., Böttcher & Liang 1999; Misra 2000; Kotov et al. 2001). These successes have warranted the construction of a detailed model ("PROPFLUC") by which the predictions can be quantitatively compared with observations, especially the shape of the power spectra at different energies as well as the time lags as functions of energy and frequency (Ingram & Done 2011, 2012; Ingram & van der Klis 2013; Rapisarda et al. 2016).

The Large Area X-ray Proportional Counter (LAXPC; P. C. Agrawal et al. 2016, in preparation ;Yadav et al. 2016a) on board the multi-wavelength satellite *AstroSat* (Agrawal 2006; Singh et al. 2014) has several advantages over the Proportional Counter Array (PCA) of *RXTE*. The effective area of LAXPC above 30 keV is significantly higher than the PCA. The event mode data obtained from LAXPC allows for the study of variations in user defined energy bins and for flux resolved spectroscopy. Finally, the various instruments on board *AstroSat* can provide wide band spectral coverage. LAXPC data of another black hole system GRS1915+105 has already revealed the capabilities of LAXPC to study high-frequency variability of high-energy photons (Yadav et al. 2016b).

Here, we report on the first analysis of LAXPC observations of Cygnus X-1 to highlight its potential to make a significant enhancement in our understanding of the system.

2. LAXPC Observations of Cygnus X-1

Figure 1 shows the 1 s binned light curve generated using data from three *AstroSat* orbits during 2016 January 8. Cygnus X-1 is detected at a level of ∼5000 c/s, except when the satellite passes through the South Atlantic Anomaly (SAA) and when the source is obscured by the earth. Data was used when the source was visible leading to an effective exposure time of 12 ks.

The spectra were extracted from each proportional counter of the LAXPC, which are named LAXPC 10, 20, and 30. The channels were grouped so that the energy bins were about 6% of the mean energy, which is roughly a third of the average spectral resolution of the detectors, i.e., ∼18%. The spectra were fitted using XSPEC version 12.8.1. The energy range considered was between 3 to 80 keV and all layers were included. The response and background files were obtained from software that would become part of the LAXPC software release (H. N. Antia et al. 2016, in preparation). The background estimates were based on observed blank skies and at present, the background estimate is approximate. Hence, its uncertainty was taken into account by adding a 5% systematic error to the error on the background rate. The uncertainties in the spectral response was taken into consideration by adding a systematic of 2% for the overall fitting. For the joint fitting of the three proportional counters, the relative normalization of LAXPC 20 and 30 were allowed to vary with respect to that of LAXPC 10. For the joint fit described below, the relative normalizations turned out to be 1.10 and 1.11 of LAXPC 30 and 20 with respect to LAXPC 10.

The typical hard state spectrum of Cygnus X-1 in the 3–80 keV is known to be described by a thermal Comptonization component with photon index $\Gamma \sim 1.8$, a moderate reflection component and a weak disk emission. These spectral components were described by the thermal Comptonization model "nthcomp," the disk black body model "diskbb" and the convolution reflection model "ireflect" in XSPEC. The seed photons for the thermal Comptonization was assumed to be from the disk. The temperature of the reflecting medium was taken to be the maximum temperature of the disk, while its abundance was fixed to solar values. The fit was found to be insensitive to the inclination angle and hence its cosine was fixed at 0.5. The spectrum above 3 keV is not sensitive to Galactic absorption and its column density was fixed to 7×10^{21} cm^{-2} (e.g., Tomsick et al. 2014) using the XSPEC model "Tbabs." The best-fit parameters obtained by the joint fitting are listed in Table 1 and the unfolded spectra with residuals are shown in Figure 2. The photon index of the primary component is ∼1.77. The upper limit of the electron temperature was not constrained, while its lower limit was 60 keV. Hence we fixed the temperature to 70 keV. A weak disk emission is technically required by the data with a flux contribution of ∼15% in the 3–5 keV band. Its temperature is ∼0.85 keV, which is significantly larger than ∼0.1 keV obtained using *Suzaku* and *Nustar* data (Table 4 of Parker et al. 2015). More importantly, its normalization of ∼200 implies a very small inner radius of a few kms for a distance of 2 kpc. This discrepancy is not unexpected since the 4–10 keV band is known to be complex with ionized absorption and relativistically blurred iron line (Parker et al. 2015). Clearly, such a detailed spectral analysis is neither warranted nor possible for an instrument with LAXPC spectral resolution, especially given that in these early stages, the response and

Table 1
Spectral Parameters

Model Parameters	Values
Γ	$1.77^{+0.006}_{-0.007}$
kT_e (keV)	70^f
$kT_{\rm disk}$ (keV)	$0.85^{+0.09}_{-0.09}$
$N_{\rm disk}$	235^{+153}_{-74}
$R_{\rm refl}$	$0.41^{+0.04}_{-0.03}$
ξ	96^{+34}_{-22}
$\rm Flux_{3-80\ keV}$ ($\times 10^{-8}$ erg s^{-1} cm^{-2})	$1.751^{+0.007}_{-0.007}$
χ^2/dof	134.2/120

Note. Γ and kT_e are the photon index and electron temperature of the thermal Comptonization component; ^{f} is the temperature, kT_e was not constrained by the data and only a lower limit of 60 keV was attained. Hence the temperature was fixed at 70 keV; $kT_{\rm disk}$ and $N_{\rm disk}$ are the normalization of the disk component; $R_{\rm refl}$ and ξ are the reflected fraction and ionization parameter of the reflected component and $\rm Flux_{3-80\ keV}$ is the unabsorbed flux in the 3–80 keV band. All errors are at the 2σ level.

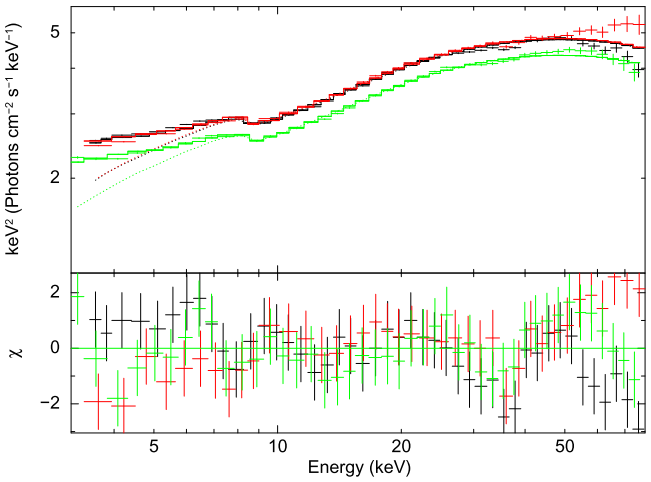

Figure 2. 3–80 keV unfolded spectra and residuals for the three LAXPC detectors—LAXPC 10 (red), LAXPC 20 (green), and LAXPC 30 (black) fitted jointly by the model whose parameters are listed in Table 1.

background are fairly uncertain. Our motivation here is to show that at this level of uncertainty in the response and background, the data is well represented by a typical hard state spectral model of Cygnus X-1. Thus, the energy dependent variability, which is the primary focus of this work, can be considered to be reliable.

We compute the power spectra for different energy bands and show the result in Figure 3 for the 3–10 and 20–40 keV bands. The light curve was divided into 702 segments, each having a length of 1024 points with a time bin of 16.67 milliseconds. The power spectrum was computed for each segment and then averaged. The resultant power spectrum was rebinned in frequency space. The dead-time-corrected Poisson noise, assuming a dead time of 42 microseconds (Yadav et al. 2016b), has been subtracted and the power spectra have been corrected for the corresponding background rates. The power spectra clearly show two broad features at ∼0.4 and ∼3 Hz and we use two broad lorentzians (e.g., Belloni et al. 2002) to empirically represent them. For the low and high-energy bands, the fit gives χ^2/dof of 130.2/52 and 92.1/51 respectively. If a systematic of 5% is added, these χ^2 values decrease to 39.4 and 52.6. Alternatively, one can instead, include two extra

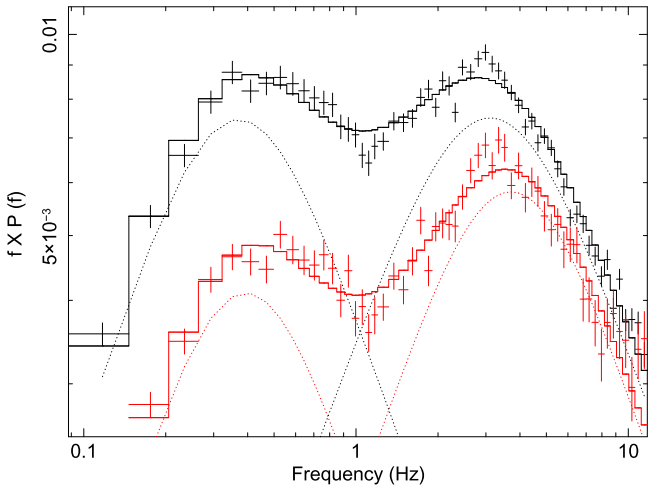

Figure 3. Frequency times the power spectra of Cygnus X-1 for photons in the 3–10 keV band (black points) and for those in the 20–40 keV band (red points). The spectra has been fitted by two lorentzian components and the figure shows the changes in the power spectral shape as a function of energy.

lorentzian components and such a fitting gives acceptable reduced χ^2 close to unity. However, in the absence of a detailed physical model for the components, in this work, we consider only the fit using two lorentzians and refer to them as the low and high-frequency components. For the low-energy band the low frequency is modeled as a lorentzian with a centroid frequency of 0.17 ± 0.04 Hz and a width of 0.65 ± 0.06 Hz. While for the high-energy band these values are found to be 0.20 ± 0.05 Hz and 0.66 ± .07 Hz. Thus marginally within errors the shape of the low-frequency component does not seem to vary. For the high-frequency component of the low-energy band the centroid frequency and width are 1.21 ± 0.3 Hz and 5.7 ± 0.2 Hz, while for the high-energy band they are 1.8 ± 0.35 Hz and 6.5 ± 0.35 Hz. Note that for a broad lorentzian the peak of the frequency times power spectrum as shown in Figure 3 occurs not at the centroid frequency f_c but at $(f_c + \sqrt{f_c^2 + (\sigma/2)^2})/2$ where σ is the width. Thus, while the shape of the low-frequency power spectral component seems to be the same with energy, there is evidence that the high-frequency ones change and peak at a higher frequency at higher energies. The strength of the components (i.e., their rms) changes with energy, especially their relative strength. This is shown more clearly in Figure 4 where the rms of the two components are plotted as a function of energy. Here, the two component lorentzian model has been fitted to the power spectra of each energy bin. Clearly, while the rms of the low-frequency component decreases rapidly with energy, that of the high-frequency one is relatively constant. We note that while there may be uncertainties on the absolute value of the rms (due to uncertainties in the actual background level), the relative strength of the two is independent of any background variation, which will effect both in the same manner.

Figure 5 shows the time lag of the high-energy 20–40 keV photons relative to the low-energy 5–10 keV band as a function of frequency. Just as in the case of the power spectra, the light curve was divided into 702 segments, each having a length of 1024 points with a time bin of 16.67 milli-secs and cross spectrum for each segment was computed and averaged. The time lags and their error were computed from the averaged cross-spectra using the scheme described in Nowak et al.

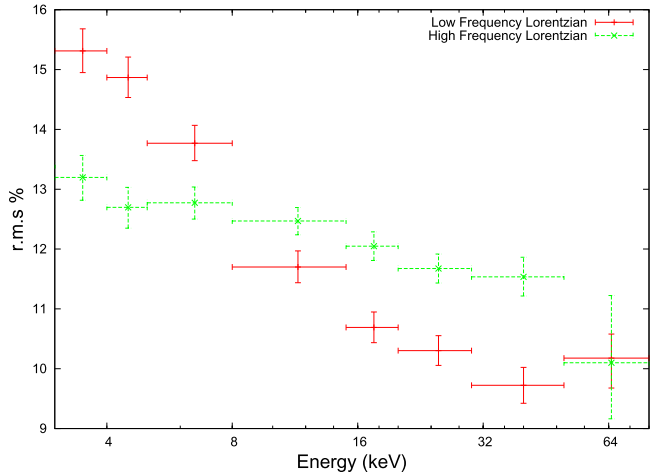

Figure 4. rms of the low- (red) and high- (green) frequency components as a function of energy. While the strength of the low-frequency components drops rapidly with energy, that of the high frequency is relatively more constant.

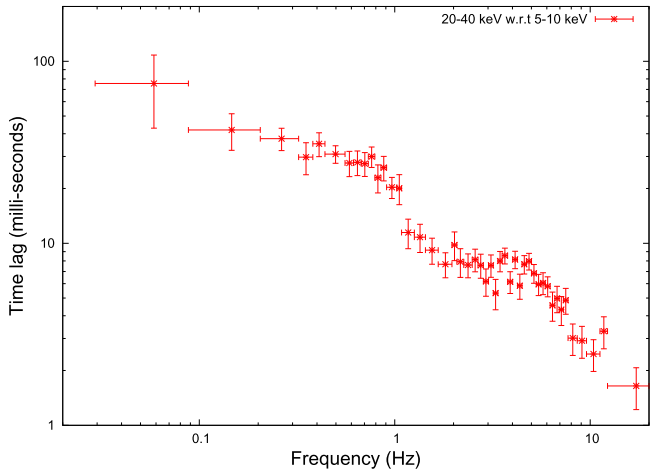

Figure 5. Time lag of the 20–40 keV photons with respect to the 5–10 keV photons as a function of frequency. The behavior seems to correspond to the power spectra shown in Figure 3.

(1999). The corresponding time lags were then rebinned in frequency space. The time lag as a function of frequency for Cygnus X-1 has been known to be roughly a power law (Nowak et al. 1999), but they were indications of complexities such as "steps" or regions in frequency space where the time lag is roughly constant. Here, the LAXPC data provides confirmation. The time lag is nearly constant between 0.05 to ∼0.9 Hz at ∼50 milliseconds and then drops to around ∼8 milliseconds in the frequency range of 2–6 Hz before finally dropping to ∼3 milliseconds at higher frequency. As indicated in the *RXTE* analysis, the time-lag behavior with frequency has a close correspondence with the power spectra at the two energy bands, in the sense that the behavior of the low- and high-frequency components are distinct.

Figure 6 shows the phase lag at the peaks of the low (∼0.4 Hz) and high (∼3 Hz) frequency components as a function of energy. Here the reference is the 5–7 keV band. The phase lags vary roughly linearly with the logarithm of the energy as has been known before (Nowak et al. 1999), except that the LAXPC data extends this relation to higher energies. It is interesting to note that there seems to be some marked difference between the low- and high-frequency behavior with

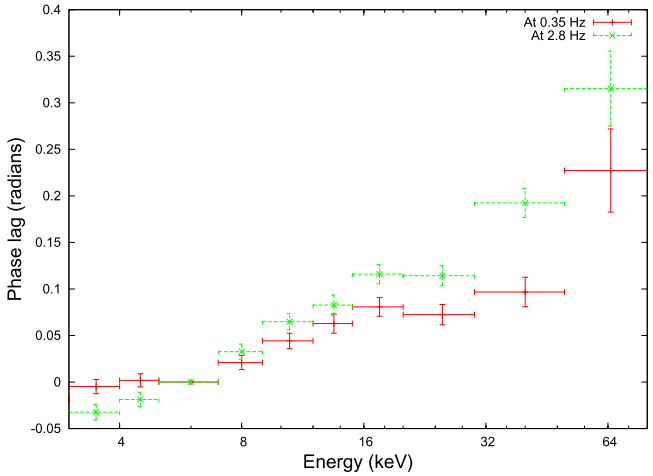

Figure 6. Phase lag (i.e., $2\pi f$ times the time lag) of the photons in different energy bands with respect to those in the 5–7 keV band for the low (∼0.35 Hz) and for the high (∼2.8 Hz) frequencies.

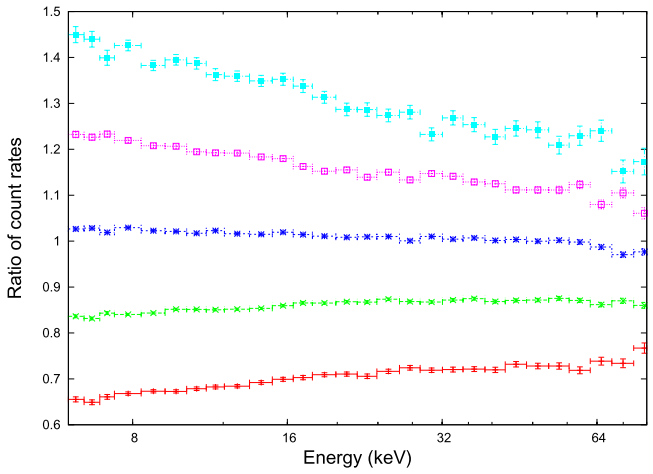

Figure 7. Count rate ratio vs. energy of flux resolved spectra at 1 s time bins normalized to the average count rate. The five spectra correspond to different fluxes corresponding to every alternate value shown in Figure 8. The spectra clearly show softening with increasing flux and with a pivot point, which is at high energies.

the time lag for low-frequency component seems to show leveling off at high energies. However, the statistics is not sufficient to make concrete statements.

The event mode data of LAXPC allows flux resolved spectroscopy at fast timescales. The power spectra shown in Figure 3 shows that a natural timescale, which demarks the low-frequency behavior from the high one, is about 1 s. The light curve binned at 1 s as shown in Figure 1 can be divided into several flux (or count rate) values, and spectroscopy can be done on each of them. Since, the spectral analysis will be dominated by systematics (rather than Poisson statistics), we consider only LAXPC 10 for the analysis. Figure 7 shows the ratio of the count rates at five different flux levels divided by the average count rates as a function of energy. Spectral evolution as the flux changes is clearly visible and specifically it can be seen that the source becomes softer as it gets brighter. The pivot point where the variability should be zero, seems to be at energies >80 keV. To quantify the spectral variation, we fitted the different flux resolved spectra with the same model used for the average one and plot the photon index versus the unabsorbed 3–80 keV unabsorbed flux in Figure 8. The photon

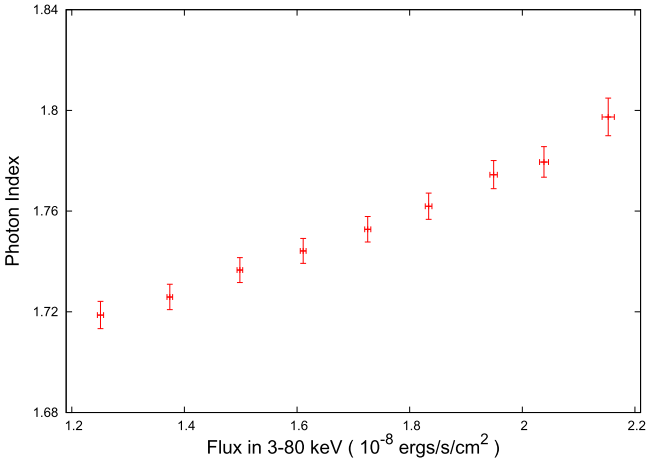

Figure 8. Photon index vs. flux for flux resolved spectra at a timescale of 1 s.

index clearly shows a correlation with flux changing by nearly 0.1 for a factor of two variation in the flux, at a remarkably fast timescale of 1 s. The variation of the other spectral parameters, such as those of the disk component, are within errors. Clearly, tighter constraints can be obtained once the background and the response of the detectors is better modeled. The analysis shows that LAXPC data can be analyzed using more sophisticated techniques like frequency resolved spectroscopy where spectra corresponding to different frequency variation are generated (Revnivtsev et al. 1999, 2000; Reig et al. 2006) and also by the alternate technique known as timescale resolved spectroscopy, where the analysis is undertaken in the time domain (Wu et al. 2009). Such an analysis can reveal spectral variations, such as that the spectral index correlates with flux for Cygnus X-1, on timescales as short as 64 msecs (Wu et al. 2010). However, these analyses have been limited to few of the *RXTE* observations taken in particular modes and even for these data the spectral information was often limited to few energy bins (Wu et al. 2009, 2010).

3. Discussion

The event mode data of LAXPC with a significantly larger effective area at energies above 30 keV than *RXTE* have provided an enhanced view of the hard X-ray variability of Cygnus X-1 in its hard state.

The timing behavior can provide clues to the geometry of the system. For example, frequency resolved spectroscopy of Cygnus X-1 in the hard state, suggests that the disk is truncated (Revnivtsev et al. 1999). Here, we discuss the results, to indicate that they are consistent with the qualitative features of the propagation fluctuation model in a geometry where the standard disk is truncated and stochastic fluctuations occur throughout the disk (and the inner hot flow) at characteristic frequencies, which propagate inward. However, it may be possible that the same broad qualititative timing features can also be produced in a geometry where the disk extends to the last stable orbit as indicated by spectral fitting of the complex iron line (Parker et al. 2015). The timing results need to be compared with detailed quantitative predictions of models with different geometry to make clear statements.

The power spectrum can be characterized as having two broad lorentzian features termed here as low (∼0.4 Hz) and high (∼3.0 Hz) frequency components. The rms of the low-frequency component decreases with energy. This is more clearly evident in the 1 s binned flux resolved spectra, which shows that the spectra soften with increasing flux. The photon index increased from 1.72 to 1.80 as the flux increased by a factor of two. Such a steepening with flux is expected if the variability is primarily due to increase in the soft photon flux. This indicates that the low-frequency variability is primarily driven by variation in the seed photon flux into the Comptonizing medium, which is likely to be the outer truncated standard disk. These low-frequency fluctuations would then propagate inward on viscous timescales causing variations in the inner corona such as in its heating rate. Thus the low-frequency variability of the thermal Comptonization component has two drivers. First, the variation of the seed photon flux (causing the spectrum to soften with increasing flux) and later after the fluctuation has reached the inner flow a variation in the overall flux of the corona. Thus one expects a time delay between the two drivers, which may show up as the observed time lag between the hard and soft X-ray photons.

For the high-frequency component, the rms decreases less rapidly with energy as compared to the soft one. Moreover, there is some evidence that the shape of the component changes with energy in the sense that its peak shifts to a higher frequency as the energy increases. The time lag between the high and andlow-energy photons is significantly smaller than the case for the low-frequency component. All this seems to indicate that the high-frequency component is driven by variations in the thermal plasma itself, i.e., it originates in the inner flow in accordance with the fluctuation propagation model.

The results presented here showcase the unprecedented view that LAXPC provides of the rapid variability properties of the X-rays above 30 keV for Cygnus X-1. Clearly, further observations of the source in different spectral states when combined with data from other instruments of *AstroSat* will allow quantitative testing of models that strive to explain variability properties of such systems and hence to constrain the dynamics of the inner accretion flow near the black hole.

We acknowledge the strong support from Indian Space Research Organization (ISRO) in various aspect of instrument building, testing, software development, and mission operation during the payload verification phase. We acknowledge support of the TIFR central workshop during the design and testing of the payload.

References

Agrawal, P. C. 2006, AdSpR, 38, 2989
Belloni, T., Psaltis, D., & van der Klis, M. 2002, ApJ, 572, 392
Böttcher, M., & Liang, E. P. 1999, ApJL, 511, L37
Gleissner, T., Wilms, J., Pottschmidt, K., et al. 2004, A&A, 414, 1091
Ingram, A., & Done, C. 2011, MNRAS, 415, 2323
Ingram, A., & Done, C. 2012, MNRAS, 419, 2369
Ingram, A., & van der Klis, M. 2013, MNRAS, 434, 1476
Kotov, O., Churazov, E., & Gilfanov, M. 2001, MNRAS, 327, 799
Liang, E. P. T., & Price, R. H. 1977, ApJ, 218, 247
Lyubarskii, Y. E. 1997, MNRAS, 292, 679
Misra, R. 2000, ApJL, 529, L95
Nowak, M. A., Vaughan, B. A., Wilms, J., Dove, J. B., & Begelman, M. C. 1999, ApJ, 510, 874
Parker, M. L., Tomsick, J. A., Miller, J. M., et al. 2015, ApJ, 808, 9
Plant, D. S., Fender, R. P., Ponti, G., Muñoz-Darias, T., & Coriat, M. 2015, A&A, 573, A120
Rapisarda, S., Ingram, A., Kalamkar, M., & van der Klis, M. 2016, MNRAS, 462, 4078
Reig, P., Papadakis, I. E., Shrader, C. R., & Kazanas, D. 2006, ApJ, 644, 424

Remillard, R. A., & McClintock, J. E. 2006, ARA&A, 44, 49
Revnivtsev, M., Gilfanov, M., & Churazov, E. 1999, A&A, 347, L23
Revnivtsev, M., Gilfanov, M., & Churazov, E. 2000, A&A, 363, 1013
Shapiro, S. L., Lightman, A. P., & Eardley, D. M. 1976, ApJ, 204, 187
Singh, K. P., Tandon, S. N., Agrawal, P. C., et al. 2014, Proc. SPIE, 9144, 91441S
Thorne, K. S., & Price, R. H. 1975, ApJL, 195, L101
Tomsick, J. A., Nowak, M. A., Parker, M., et al. 2014, ApJ, 780, 78
Uttley, P., & McHardy, I. M. 2001, MNRAS, 323, L26
Uttley, P., McHardy, I. M., & Vaughan, S. 2005, MNRAS, 359, 345
Wilms, J., Pottschmidt, K., Nowak, M. A., et al. 2004, NuPhS, 132, 420
Wu, Y. X., Belloni, T. M., & Stella, L. 2010, MNRAS, 408, 2413
Wu, Y. X., Li, T. P., Belloni, T. M., Wang, T. S., & Liu, H. 2009, ApJ, 695, 921
Yadav, J. S., Agrawal, P. C., Antia, H. M., et al. 2016a, Proc. SPIE, 9905, 99051D
Yadav, J. S., Misra, R., Verdhan Chauhan, J., et al. 2016b, ApJ, 833, 27